ELSEVIER

Engineering Analysis with Boundary Elements 31 (2007) 50–65

ENGINEERING ANALYSIS with BOUNDARY ELEMENTS

www.elsevier.com/locate/enganabound

Stress intensity factors of square crack inclined to interface of transversely isotropic bi-material

Z.Q. Yue[a,*], H.T. Xiao[a], E. Pan[b]

[a]*Department of Civil Engineering, The University of Hong Kong, Pokfulam Road, Hong Kong, PR China*
[b]*Department of Civil Engineering, University of Akron, Akron, OH 44325-3905, USA*

Received 6 November 2005; accepted 6 July 2006
Available online 17 October 2006

Abstract

This paper analyzes a square crack in a transversely isotropic bi-material solid by using dual boundary element method. The square crack is inclined to the interface of the bi-material. The fundamental solution for the bi-material solid occupying an infinite region is incorporated into the dual boundary integral equations. The square crack can have an arbitrary angle with respect to the plane of isotropy of the bi-material occupying either finite or infinite regions. The stress intensity factor (SIF) values of the modes I, II, and III associated with the square crack are calculated from the crack opening displacements. Numerical results show that the properties of the anisotropic bi-material have evident influences on the values of the three SIFs. The values of the three SIFs are further examined by taking into account the effect of the external boundary of the internally cracked bi-material.

Keywords: Fracture mechanics; Dual boundary element method; Transverse isotropy; Bi-material; Fundamental solutions; Stress intensity factor

1. Introduction

Solid bi-materials can be anisotropic and inhomogeneous and can contain flaws or cracks in their internal regions. Such bi-materials are used for important structural components but can also be responsible for failures. The theoretical capability to accurately predict and calculate the responses of such bi-materials under external loading is important in engineering design and education. Therefore, over the last few decades, a large number of researchers have devoted their time and effort to develop and enhance the theoretical capability for the prediction and evaluation of anisotropic bi-materials under external loads.

Sih et al. [1] published one of their classical results on cracks in rectilinearly anisotropic materials. They found that an elastic singularity of the order $\sqrt{r}$ is always present at the crack front in a body with rectilinear anisotropy and the magnitude of the local stresses may be described in terms of stress intensity factors (SIFs). Some approaches to analyze cracks in anisotropic materials can be also found in Sih and Chen [2]. For three-dimensional cracks in anisotropic materials, Hoenig [3] derived the SIFs in terms of compact line integral expressions for an elliptical crack in an infinite anisotropic material, where the crack surface is not parallel to the plane of material isotropy. Pan and Yuan [4] analyzed a square-shaped crack in an anisotropic material by utilizing the dual boundary element method (DBEM) and presented the SIF results. On the other hand, for a rectangular crack terminating at the interface of an isotropic bi-material, Qin and Noda [5] evaluated the SIF values by using the hypersingular integral equation. However, the studies of the SIF values for the rectangular crack in anisotropic solids are still very limited, in particular for rectangular cracks in transversely isotopic bi-materials.

Yue et al. [6,7] investigated the fracture mechanics of elliptical and penny-shaped cracks in transversely isotropic bi-materials by using the multi-region methods and traction singular elements of the boundary element method (BEM). The fundamental solution of two joined transversely isotropic solids given in Yue [8] was incorporated into the traditional BEM. The traction singular element models the singularity only along one direction towards the crack

*Corresponding author. Tel.: +852 2859 1967; fax: +852 2559 5337.
E-mail address: yueqzq@hkucc.hku.hk (Z.Q. Yue).

0955-7997/$ - see front matter © 2006 Elsevier Ltd. All rights reserved.
doi:10.1016/j.enganabound.2006.07.006

front. Hence, this type of singular elements cannot handle the rectangular crack effectively.

The DBEM can be used as a general and computationally efficient way to model crack problems in elastic solids [9, 10]. Some investigators incorporated the fundamental solutions for a transversely isotropic solid [11] into the DBEM for the analysis of crack problems [4, 12]. Evidently, when the BEM associated with Pan and Chou's solution is used for the analysis of crack problems in composite materials or bi-materials, the interface between two different materials has to be discretized.

In this paper, we develop a single-domain DBEM for three-dimensional linear elastic fracture mechanics in a transversely isotropic bi-material occupying either a finite space or an infinite space. The fundamental solutions for two joined transversely isotropic solids [8] are incorporated into the single-domain DBEM formulation. The displacement and/or traction are used as unknown variables on the non-crack boundary. The crack opening displacements (CODs) are treated as unknown quantities on the crack surface. No double nodes are required along the crack surface. Different types of elements are employed to discretize the non-crack boundary and crack surface. The rigid-body motion method and the Kutt's numerical quadrature are used to calculate the strongly singular integral and the hypersingular integral, respectively. Special interpolation functions of the CODs are adopted to capture the specific characteristics of the CODs near a crack-front. The CODs obtained by the DBEM are then used to calculate the SIF values.

The proposed DBEM is applied to examine a square crack in a transversely isotropic bi-material solid (Fig. 1). The SIF values obtained with the present method are in very good agreement with existing numerical results. Two types of transversely isotropic materials are considered, resulting in four cases for the combinations of bi-material. The square crack can be oriented at different angles with respect to the plane of isotropy (i.e., the plane of bi-material interface). Numerical results illustrate the influence of the material anisotropy and the four material combinations on the SIF values. Furthermore, the square crack in a transversely isotropic bi-material occupying an infinite space is analyzed. The effect of the external boundary is therefore examined by comparing the results of the SIF values for the square in a finite cube with those in the infinite space.

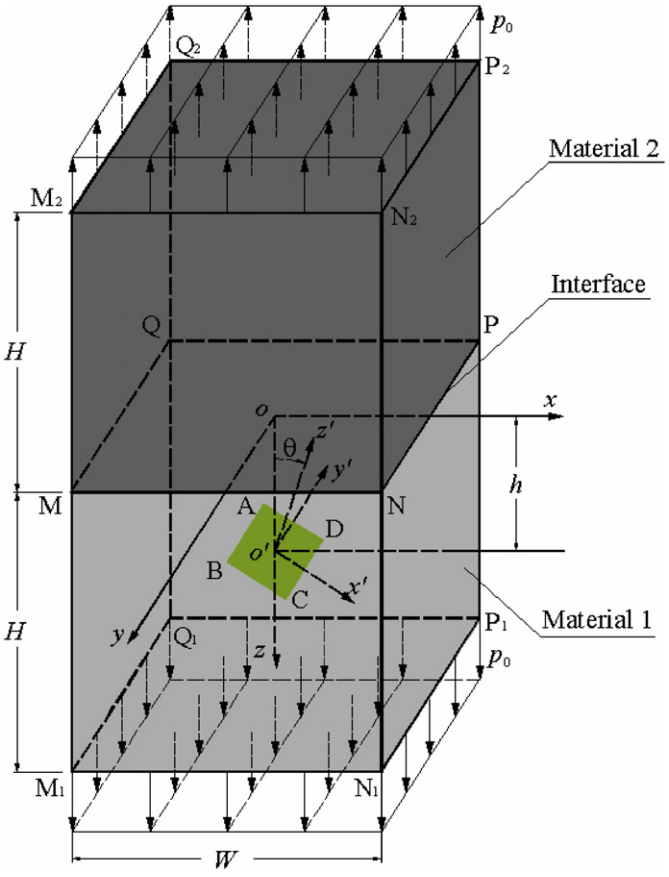

Fig. 1. A square crack (ABCD: $2c \times 2c$) in a transversely isotropic bi-material occupying a finite cube ($2H \times W \times W$).

2. DBEM for cracks in transversely isotropic bi-materials

2.1. Fundamental solutions for transversely isotropic bi-materials

Yue [8] presented the closed-form fundamental solution for the elastic field of two joined transversely isotropic solids subject to concentrated point body forces. The two solids occupy an infinite space. The interface is planar, perfectly bonded and parallel to the isotropic planes of the two transversely isotropic materials. The classical theory of Fourier integral transform was employed to solve the partial differential equations governing the response of the two joined transversely isotropic solids subject to the concentrated body-forces. The fundamental solution of displacements and stresses is presented in the forms of the elementary harmonic functions. Details of the solution can be found in Yue [8].

2.2. Square crack in a finite cube of transversely isotropic bi-material

As shown in Fig. 1, the finite cube is bounded by the six planes passing through the eight points M_1, N_1, P_1, Q_1, M_2, N_2, P_2, and Q_2. Material 1 occupies the cubic space confined by the six planes passing through the eight points M_1, N_1, P_1, Q_1, M, N, P, and Q. Material 2 occupies the cubic space confined by the six planes passing through the eight points M_2, N_2, P_2, Q_2, M, N, P, and Q. The bonded interface of the materials 1 and 2 is the plane surface MNPQ. Materials 1 and 2 are modeled as two transversely isotropic elastic solids with different elastic constant values. Their planes of isotropy are parallel to the interface of the bi-material.

A global Cartesian coordinate system *oxyz* is set up for the DBEM examination. The global system has its horizontal plane *oxy* on the interface of the bi-material and its vertical axis *z* perpendicular to the interface. The origin *o* is the projection of the center of the square crack ABCD along the *z*-axis onto the horizontal plane *oxy*. The *y*-axis is parallel to the square crack. The *x*-axis has an inclination angle θ with the square crack. A local Cartesian coordinate system $o'x'y'z'$ is also set up for the inclined square crack and has its origin o' at the crack center. The z'-axis is perpendicular to the square crack. The x'-axis is on the crack plane and parallel with the lines AD and BC of the square crack. The y'-axis is also on the crack plane and parallel with the lines AB and CD and the *y*-axis.

2.3. Dual boundary integral equations for transversely isotropic bi-materials

To incorporate Yue's fundamental solutions into the boundary integral equation formulation, we utilize the DBEM. However, in the present DBEM, the displacements and/or tractions are used as unknown variables on the non-crack boundary while the COD are chosen as the unknowns on the crack surface. This approach can avoid the use of double nodes [13, 14].

For this crack problem (Fig. 1), the non-crack boundary S consists of the following six surfaces: the top surface $P_2Q_2M_2N_2$, the bottom surface $P_1Q_1M_1N_1$, the vertical surfaces $M_2N_2N_1M_1$, $P_2Q_2Q_1P_1$, $M_2Q_2Q_1M_1$, and $N_2P_2P_1N_1$. The crack surfaces Γ (i.e., the square area ABCD) consist of the surfaces Γ^+ $(z'=0^+)$ and Γ^- $(z'=0^-)$ in the local coordinate system $o'x'y'z'$. Accordingly, in the numerical formulation, the traction equilibrium $t_j(\mathbf{x}_{\Gamma^+}) = -t_j(\mathbf{x}_{\Gamma^-})$ is assumed on the crack surfaces. The crack opening and sliding displacements are expressed as $\Delta u_j(\mathbf{x}_{\Gamma^+}) = u_j(\mathbf{x}_{\Gamma^+}) - u_j(\mathbf{x}_{\Gamma^-})$, where $j = 1$, 2 or 3.

When the body forces are absent, the displacement BIE using Yue's fundamental solution can be expressed as follows:

$$C_{ij}(\mathbf{y}_S)u_j(\mathbf{y}_S) + \int_S t^*_{ij}(\mathbf{y}_S,\mathbf{x}_S)u_j(\mathbf{x}_S)\,\mathrm{d}S(\mathbf{x}_S) + \int_{\Gamma^+} t^*_{ij}(\mathbf{y}_S,\mathbf{x}_{\Gamma^+})\Delta u_j(\mathbf{x}_{\Gamma^+})\,\mathrm{d}\Gamma(\mathbf{x}_{\Gamma^+}) = \int_S u^*_{ij}(\mathbf{y}_S,\mathbf{x}_S)t_j(\mathbf{x}_S)\,\mathrm{d}S(\mathbf{x}_S), \tag{1}$$

where

- $i = 1$, 2 or 3;
- $\mathbf{y}_S$ and $\mathbf{x}_S$ denote the source and field points, respectively;
- $u_j(\mathbf{y}_S)$ and $t_j(\mathbf{y}_S)$ are the displacements and tractions on the non-crack boundary S, respectively;
- $\Delta u_j(\mathbf{x}_{\Gamma^+})$ is the COD on the crack surface;
- $u^*_{ij}(\mathbf{y}_S,\mathbf{x}_S)$ and $t^*_{ij}(\mathbf{y}_S,\mathbf{x}_S)$ are the fundamental displacements and tractions of Yue's solution, respectively; and
- $C_{ij}(\mathbf{y}_S)$ is a coefficient matrix dependent on the local boundary geometry at the source point $(\mathbf{y}_S)$. The $C_{ij}(\mathbf{y}_S)$ can be evaluated using the following equation:

$$C_{ij}(\mathbf{y}_S) = \lim_{\varepsilon\to 0}\int_{S_\varepsilon} t^*_{ij}(\mathbf{y}_S,\mathbf{x}_S)\,\mathrm{d}S(\mathbf{x}_S), \tag{2}$$

where S_ε is an infinitesimal spherical surface with center at $\mathbf{y}_S$ and radius of ε enclosed in the solids.

Assume that $\mathbf{y}_{\Gamma^+}$ is a smooth point on the crack surface Γ^+. The traction BIE can be expressed as

$$t_i(\mathbf{y}_{\Gamma^+}) + n_j(\mathbf{y}_{\Gamma^+})\int_S T^*_{ijk}(\mathbf{y}_{\Gamma^+},\mathbf{x}_S)u_k(\mathbf{x}_S)\,\mathrm{d}S(\mathbf{x}_S) + n_j(\mathbf{y}_{\Gamma^+})\int_{\Gamma^+} T^*_{ijk}(\mathbf{y}_{\Gamma^+},\mathbf{x}_{\Gamma^+})\,\Delta u_k(\mathbf{x}_{\Gamma^+})\,\mathrm{d}\Gamma(\mathbf{x}_{\Gamma^+}) = n_j(\mathbf{y}_{\Gamma^+})\int_S U^*_{ijk}(\mathbf{y}_{\Gamma^+},\mathbf{x}_S)t_k(\mathbf{x}_S)\,\mathrm{d}S(\mathbf{x}_S), \tag{3}$$

where

- $n_j(\mathbf{y}_{\Gamma^+})$ is the unit outward normal of the positive side of the crack surface at $\mathbf{y}_{\Gamma^+}$;
- $U^*_{ijk}(\mathbf{y}_{\Gamma^+},\mathbf{x}_S)$ and $T^*_{ijk}(\mathbf{y}_{\Gamma^+},\mathbf{x}_S)$ are the new kernel functions of Yue's fundamental solution.

It is noted that the traction BIE (3) is valid if the following conditions are held [15]:

- the local geometry at the source point is smooth,
- the displacement derivative field is Hölder continuous, and
- the traction field is Hölder continuous.

If the crack surface possesses discontinuous tangential planes either at certain points or along certain lines, the numerical execution of the traction BIE needs to be carried out carefully. The most general strategy to satisfy the three conditions on the crack surface involves the use of discontinuous elements where the source points are moved to the interior of the discontinuous elements.

A numerical scheme is further presented below for calculating the new kernel functions U^*_{ijk} and T^*_{ijk} by using the displacements u^*_{ij} and the tractions t^*_{ij}. For a transversely isotropic elastic solid, the constitutive relation between the stresses σ_{ij} and the strains ε_{mn} can be expressed as

$$\sigma_{ij} = C_{ijmn}\varepsilon_{mn}, \tag{4}$$

where C_{ijmn} is the fourth-order stiffness tensor of the transversely isotropic elastic solid and its elements are given in Eq. (A1) of Appendix A.

In Eq. (3), the kernel functions U^*_{ijk} and T^*_{ijk} can be written as

$$U^*_{ijk} = \frac{1}{2}C_{ijmn}\left(u^*_{mk,n} + u^*_{nk,m}\right), \tag{5a}$$

$$T^*_{ijk} = \frac{1}{2}C_{ijmn}\left(t^*_{mk,n} + t^*_{nk,m}\right). \tag{5b}$$

In Eqs. 5(a,b), the derivatives of Yue's tractions and displacements can be replaced by the numerical difference of the corresponding ones. In other words, for U^*_{ijk}, we employ the following formulae:

$$\frac{\partial u^*_{ik}}{\partial x_1} \approx \frac{1}{2d}\left[u^*_{ik}(x_1+d,x_2,x_3) - u^*_{ik}(x_1-d,x_2,x_3)\right], \tag{6a}$$

$$\frac{\partial u^*_{ik}}{\partial x_2} \approx \frac{1}{2d}\left[u^*_{ik}(x_1,x_2+d,x_3) - u^*_{ik}(x_1,x_2-d,x_3)\right], \tag{6b}$$

$$\frac{\partial u^*_{ik}}{\partial x_3} \approx \frac{1}{2d}\left[u^*_{ik}(x_1,x_2,x_3+d) - u^*_{ik}(x_1,x_2,x_3-d)\right]. \tag{6c}$$

The derivatives of the traction, T^*_{ijk}, can also be expressed similarly in terms of the numerical difference of t^*_{ik}.

In order to obtain T^*_{ijk} and U^*_{ijk} at the source point $\mathbf{y}(x_1, x_2, x_3)$ and the field point $\mathbf{x}$, it is necessary to compute the fundamental solutions at six points in the neighborhood of $\mathbf{y}(x_1, x_2, x_3)$. Clearly, the choice of the interval d in Eq. (6) is the key factor for the accuracy of this approximation. As shown independently by us in Section 3, the best value of the interval for the two jointed transversely isotropic solids is

$$d = r \times 10^{-6}, \tag{7}$$

where r is the distance between the field and source point. This is in consistence with Tonon et al. [16] where they verified expression (7) for the general anisotropic materials.

When the above DBEM is utilized to solve the crack problem in an infinite extent, the displacement BIE (1) is not needed. Therefore, the traction BIE (3) is reduced to that associated with the displacement discontinuous method (DDM; e.g., [17,18]):

$$t_i(\mathbf{y}_{\Gamma^+}) + n_j(\mathbf{y}_{\Gamma^+}) \int_S T^*_{ijk}(\mathbf{y}_{\Gamma^+}, \mathbf{x}_{\Gamma^+}) \Delta u_k(\mathbf{x}_{\Gamma^+})\, \mathrm{d}\Gamma(\mathbf{x}_{\Gamma^+}) = 0. \tag{8}$$

It is remarked that, if needed, the actual crack surface displacements can be retrieved using expression (1) to collocate on one side of the crack surfaces, say on Γ^- to obtain u^-_j [19]. The opposite crack surface u^+_j can therefore be easily obtained by using the relations $u^+_j = \Delta u_j + u^-_j$.

Eqs. (1) and (3) do not contain the integrations on the bi-material interface because Yue's fundamental solutions strictly satisfy the interface conditions of two joined transversely isotropic solids. Eqs. (1) and (3) can be discretized to obtain a set of linear system of equations for the solution of the unknown displacements, tractions and the CODs.

2.4. Numerical methods of dual boundary integral equations

In the present DBEM, the eight-node isoparametric elements are used to discretize the non- crack boundary. The shape functions of the eight-node isoparametric elements were presented in Lachat and Watson [20]. Because the kernel functions need to be evaluated repeatedly, significant saving in CPU time can be realized by coding the arithmetic efficiently. In the computer code of the present DBEM, the adaptive integration scheme in Gao and Davies [21] is employed.

To discretize the crack surface, the three types of nine-node elements proposed by Pan and Yuan [4] are adopted. The isoparametric elements and two types of the discontinuous elements, as shown in Fig. 2, are used. The coordinates at any point in an element are then related to its element nodal coordinates as follows:

$$x_i = \sum_{l=1}^{9} \phi_l x^l_i, \quad i = 1,2,3, \tag{9}$$

where $\phi_l (l = 1{-}9)$ are the shape functions of the boundary elements. Detailed expressions for $\phi_l (l = 1{-}9)$ can be found in [4].

For the positions on the crack surface and far away from the crack front, the nine-node isoparametric element is used to discretize the surface. The CODs are approximated by their nodal values, and can be expressed as

$$\Delta u_i = \sum_{l=1}^{9} \phi_l \Delta u^l_i, \quad i = 1,2,3, \tag{10}$$

where $\phi_l (l = 1{-}9)$ are the shape functions and Δu^l_i the CODs at nodal point l.

In order to capture the specific characteristics of the CODs near a crack front, two kinds of discontinuous quadrilateral elements (types I and II) are employed. The CODs of the element type I, as shown in Fig. 2a, are approximated by their nodal values as

$$\Delta u_i = \sum_{l=1}^{9} \sqrt{1+\eta}\,\phi_l \Delta u^l_i, \quad i = 1,2,3, \tag{11}$$

where $\phi_l (l = 1{-}9)$ are the shape functions and Δu^l_i the nodal CODs at nodal point l. The coefficient $\sqrt{1+\eta}$ is introduced in Eq. (11) to capture the crack behavior at the crack front. This type of elements is positioned at the smooth crack front.

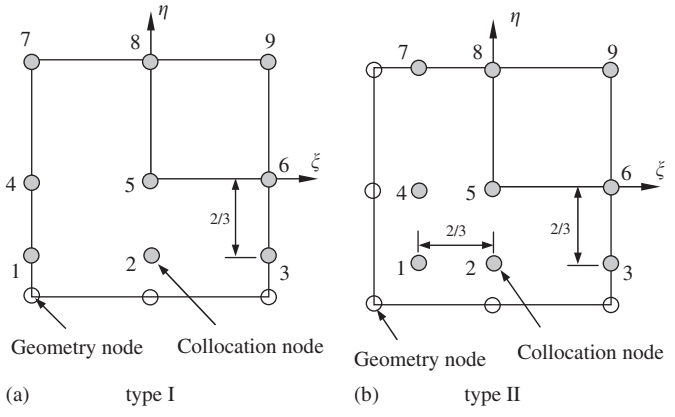

Fig. 2. Two types of singular elements.

The CODs of the element type II, as shown in Fig. 2b, are approximated as

$$\Delta u_i = \sum_{l=1}^{9} \sqrt{1+\xi}\sqrt{1+\eta}\phi_l \Delta u_i^l, \quad i = 1,2,3, \tag{12}$$

where $\phi_l (l = 1-9)$ are the shape functions and Δu_i^l the nodal CODs at nodal point l. This type of elements is positioned at the non-smooth crack front. Similarly, the coefficient $\sqrt{1+\xi}\sqrt{1+\eta}$ in Eq. (12) is used to capture the crack behavior at the crack front.

2.5. The numerical method for strongly singular and hypersingular integrals

In the displacement BIE (1), the weakly singular integrals $o(r^{-1})$ can be solved by the coordinate transform [20]. These methods were also used for the analysis of three-dimensional (3D) crack problems in multilayered solids [22]. In Eq. (1), the second term on the left-hand side of Eq. (1) has a strong singularity $o(r^{-2})$. These strongly singular integrals and the coefficients $C_{ij}(\mathbf{y}_S)$ can be calculated by the rigid-body motion method employed in the conventional displacement BIE [4].

The traction BIE (3) has the following integral with a high singularity $o(r^{-3})$:

$$\int_\Gamma T^*_{ijk}\left(\mathbf{y}_{\Gamma^+}, \mathbf{x}_{\Gamma^+}\right) \Delta u_k(\mathbf{x}_{\Gamma^+})\, \mathrm{d}\Gamma(\mathbf{x}_{\Gamma^+}). \tag{13}$$

The expression (13) can further be re-written as

$$\int_{-1}^{1}\int_{-1}^{1} T^*_{ijk}[\mathbf{y}(\xi^c,\eta^c), \mathbf{x}(\xi,\eta)]\phi_l(\xi,\eta) g(\xi,\eta) J(\xi,\eta)\, \mathrm{d}\xi\, \mathrm{d}\eta, \tag{14}$$

where

- (ξ^c,η^c) and (ξ,η) are the local coordinates of the source point $\mathbf{y}$ and the field point $\mathbf{x}$, respectively;
- J is the Jacobian transformation;
- For the nine-node isoparametric element, $g(\xi,\eta) = 1$;
- For the element type I, $g(\xi,\eta) = \sqrt{1+\eta}$; and
- For the element type II, $g(\xi,\eta) = \sqrt{1+\xi}\sqrt{1+\eta}$.

As Pan and Yuan [4], the numerical quadrature in Kutt's [23,24] is adopted to carry out the hypersingular integrals in Eq. (14). Introducing the polar coordinate transformation

$$\begin{aligned} \xi &= \xi^c + r\cos\vartheta, \\ \eta &= \eta^c + r\sin\vartheta. \end{aligned} \tag{15}$$

Eq. (14) can thus be re-written as

$$\sum_m \int_{\vartheta_1}^{\vartheta_2}\int_0^{R(\vartheta)} T^*_{ijk}[\mathbf{y}(\xi^c,\eta^c), \mathbf{x}(r,\vartheta)]\phi_l(r,\vartheta) g(r,\vartheta)\mathbf{J}(r,\vartheta) r\, \mathrm{d}r\, \mathrm{d}\vartheta, \tag{16}$$

where the summation over m is for all the triangles on the element as discussed below.

- If the collocation point is one of the corner points of the element, the element is then divided into two triangles, and the summation on m in expression (16) is from 1–2.
- If the collocation point is a point on the side of the square, the element needs to be divided into three triangles, and the summation on m in expression (16) is from 1–3.
- If the collocation point is an internal point, the element needs to be divided into four triangles, and the summation on m in expression (16) is from 1–4.

Now, it can be observed that the integrand is of the singularity $o(r^{-2})$. The numerical quadrature in Kutt [23, 24] can be utilized to evaluate the inner finite-part integral with respect to r. On the other hand, the outer integral with respect to ϑ is regular and can be calculated by the regular Gaussian quadrature.

For a given Gaussian point ϑ_j, the inner integral in Eq. (16) can be approximated by N-point equi-space quadrature [23,24] as follows:

$$\int_0^R \frac{f(r)}{r^2}\mathrm{d}r \approx \frac{1}{R}\sum_{i=1}^{N}(w_i + c_i \ln R) f\left(\frac{\mathrm{i}-1}{N}R\right), \tag{17}$$

where w_i are the weights and c_i the coefficients given by [23, 24], and the integrand is given by

$$\begin{aligned} f(r) = {} & T^*_{ijk}\left[\mathbf{y}(\xi^c,\eta^c), \mathbf{x}\left(r,\vartheta_j\right)\right] \\ & \times \phi_l\left(r,\vartheta_j\right) g\left(r,\vartheta_j\right) J\left(r,\vartheta_j\right) r^3. \end{aligned} \tag{18}$$

It is pointed out that when deriving the N-point equi-space quadrature (18), it has been assumed that the integrand $f(r) \in C^0[0,R]$ and $f(r) \in C^2$ in the neighborhood of $r = 0$.

If the crack surface is flat, continuous elements can be used to discretize the interior crack surface, with discontinuous elements for the crack front only. However, if the crack surface is curved, then discontinuous elements are needed for the whole crack surface in order to satisfy the continuity requirement for $f(r)$. In the following numerical examples, Kutt's 20-point equispace quadrature is used in the finite-part integral with respect to r, and 20 Gaussian points for the regular outer integral with respect to ϑ_j.

2.6. Calculation of SIFs

According to Kassir and Sih [25], there is an asymptotic relation between the CODs near the crack front and the SIF values for cracked transversely isotropic solid. Using the leading terms of those relations, the SIF values can be evaluated from the three components of the CODs at a point close to the crack front.

Ariza and Dominguez [12] presented the formulae for calculating the SIF values of a transversely isotropic solid. Pan and Yuan [4] used an extrapolation technique of the

CODs for calculating the SIF values. This technique also requires an asymptotically analytical expression of the crack-front CODs in terms of SIF values. It can use the CODs at any point to calculate the SIF values. The following formula proposed by Pan and Yuan [4] is adopted to calculate the SIF values.

Let (x_1, x_2, x_3) be a local Cartesian coordinate system attached to the crack front. The x_1-axis is normal to the crack surface. The x_3-axis is tangential to the crack front. The x_2-axis is thus formed by the intersection of the plane normal to the crack front and the plane tangential to the crack plane. The CODs can be defined as

$$\Delta u_i(x_1, x_2, x_3) = u_i^+(x_1, x_2, x_3) - u_i^-(x_1, x_2, x_3), \quad i = 1, 2, 3 \tag{19}$$

where the superscripts $^+$ and $^-$ correspond to the crack surfaces whose normal directions are $n = +1$ and $n = -1$ for the local coordinate system attached to the crack front, respectively.

It is further assumed that the crack front is smooth. The leading singular term in the asymptotic expansions of the stress and displacement fields near the crack front are amenable to the generalized plane strain analysis. Therefore, the relation of the CODs at a distance r behind the crack front and the SIFs can be expressed as [26]

$$\Delta \mathbf{u} = 2\sqrt{\frac{2r}{\pi}}\mathbf{L}^{-1}\mathbf{k}, \tag{20}$$

where $\Delta \mathbf{u} = (\Delta u_1, \Delta u_2, \Delta u_3)^{\mathrm{T}}$, and $\mathbf{k} = (K_{\mathrm{I}}, K_{\mathrm{II}}, K_{\mathrm{III}})^{\mathrm{T}}$ are the SIFs for modes I, II and III; $\mathbf{L}$ is one of the Barnett-Lothe tensors [26] depending only on the anisotropic properties of the solids in the local crack-front coordinates.

On the crack-front element, equating the CODs from the numerical calculation to the analytical expression (20), one then obtains a set of algebraic equations. From these equations, the values of the SIF K_{I}, K_{II}, and K_{III} can be obtained.

3. Numerical verifications

In the following, a square crack (the side length $2c$) in an infinite extent is studied for the verification of the accuracy of the proposed method. For this crack problem, only BIE (3) or (8) is needed. The crack surface is parallel to the plane of the isotropy in a transversely isotropic solid. The upper and lower surfaces of the crack are subject to a uniform tension p_0. One hundred (10×10) nine-node elements are used to discretize the crack surface. Among these elements, there are 64 nine-node isoparametric elements, 32 discontinuous elements of type I, and four discontinuous elements of type II. Fig. 3 shows the discretization of the crack surface (ABCD), where the eight corner points (M1 to Q2) of the cube are extended to infinity.

For the square crack in a transversely isotropic solid of infinite extent, the SIF values are the same as those for the isotropic case, i.e., independent of material properties. Weaver [18] obtained the SIF values of the rectangular crack in an isotropic solid of infinite extent by the discontinuous displacement method. The maximum value occurs at the middle of the square side and decrease to zero at the corner. The maximum normalized SIF value ($K_I/p_0\sqrt{\pi c}$) predicted from the present DBEM is 0.7605. This value is compared well with the value of 0.74 in Weaver [18], the value of 0.76 in Murakami [27] for isotropic solids and the value of 0.7626 in Pan and Yuan [4].

In order to obtain the best value d in expression (7), five values of d are used. They are $10^{-4}r$, $10^{-5}r$, $10^{-6}r$, $10^{-7}r$ and $10^{-8}r$, respectively. For the five values of d, the maximum normalized SIF values ($K_I/p_0\sqrt{\pi c}$) at the middle

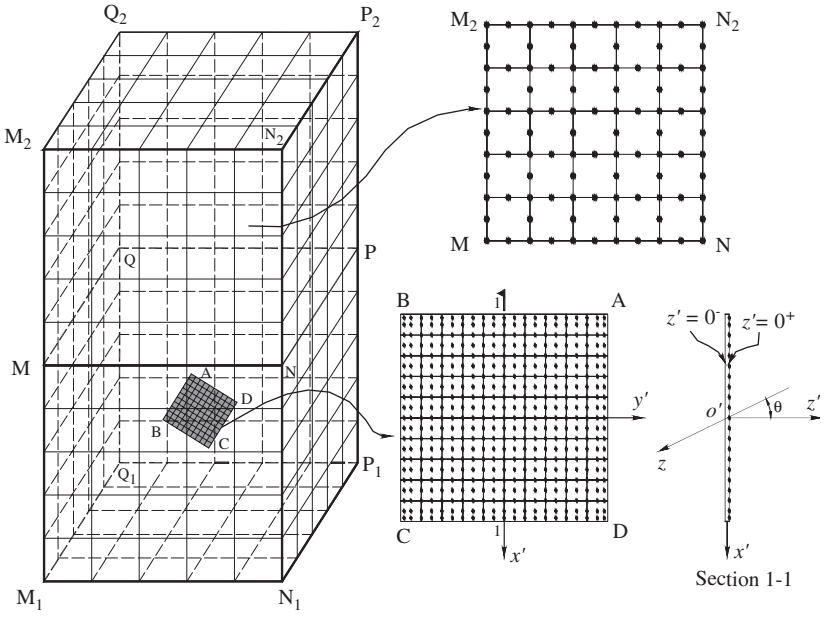

Fig. 3. Boundary element mesh of the cracked finite cube.

of the square side are equal to 0.7250, 0.7503, 0.7605, 0.7748, and 0.6661, respectively. These results may verify that the d value in Eq. (7) is suitable for the present analysis.

4. Applications

The present DBEM is used to calculate the SIF values of the square crack in the transversely isotropic bi-material (Fig. 1). The bi-material occupies either finite cube or infinite space.

4.1. Material properties

As shown in Fig. 1, the oxy plane is the isotropic plane of the two joined transversely isotropic materials 1 and 2 and the z-axis is the normal axis of material isotropy. Each of the materials 1 and 2 has the elastic constants E_x, μ_x, v_{xy}, E_z, μ_z, and v_{xz}. The E_x, μ_x, and v_{xy} are the Young's modulus, shear modulus, and Poisson's ratio in the oxy plane of isotropy, respectively. The E_z, μ_z, and v_{xz} are the corresponding quantities in the transverse direction z, respectively. The five elastic constants c_{ik} ($i = 1, 2, 3, 4, 5$; $k = 1, 2$) in Eq. (A1) have the following relations with the elastic constants E_x, μ_x, v_{xy}, E_z, μ_z, and v_{xz}:

$$E_x = 4c_{5k}\frac{\left(c_{1k}c_{3k} - c_{5k}c_{3k} - c_{2k}^2\right)}{\left(c_{1k}c_{3k} - c_{2k}^2\right)}, \tag{21a}$$

$$\mu_x = c_{5k}, \tag{21b}$$

$$v_{xy} = \tfrac{1}{4}E_x\frac{\left(c_{1k}c_{3k} - 2c_{3k}c_{5k} - c_{2k}^2\right)}{c_{5k}/\left(c_{1k}c_{3k} - c_{5k}c_{3k} - c_{2k}^2\right)}, \tag{21c}$$

$$E_z = \frac{\left(c_{1k}c_{3k} - c_{5k}c_{3k} - c_{2k}^2\right)}{\left(c_{1k} - c_{5k}\right)}, \tag{21d}$$

$$\mu_z = c_{4k}, \tag{21e}$$

$$v_{xz} = \frac{1}{2}E_z c_{2k}/\left(c_{1k}c_{3k} - c_{5k}c_{3k} - c_{2k}^2\right), \tag{21f}$$

where $k = 1$ for $0^+ \leqslant z < \infty$ and 2 for $-\infty < z \leqslant 0^-$.

Table 1
Elastic constants of the two transversely isotropic solids

Material types	c_1	c_2	c_3	c_4	c_5	E_x/E_z
Rhenium (GPa)	61.2	20.6	68.3	16.2	17.1	0.8032
Cadmium (GPa)	11.6	4.14	5.1	1.95	3.685	2.7764

In the present study, two transversely isotropic materials (i.e., rhenium and cadmium, Lin and Keer, [28]) are selected for the numerical evaluation. Elastic constants of these two materials are listed in Table 1. Accordingly, there are four different cases of the material combinations for the bi-material (Table 2).

4.2. A square crack in a transversely isotropic bi-material of finite cubic space

4.2.1. General conditions

Fig. 1 shows the square crack in a transversely isotropic bi-material occupying a finite cubic space. The finite cube with a square crack is subject to a uniform tension p_0 at the top and bottom faces along the z-axis direction.

The cube has a height $2H$ and width W. In particular, $W = 4c$ and H. The side length of the inclined square crack ABCD is $2c$. The origin of the global coordinate system $oxyz$ is located at the center of the bi-material interface of the cube. The origin o' and the crack center are located at the same point $(0, 0, h)$ in the global coordinate system. Without loss of generality, the square crack is always located in the material 1 ($z \geqslant 0^+$) for the cases under consideration.

For this crack problem, both BIEs (1) and (3) are needed. The boundary element mesh of the cracked finite cube is shown in Fig. 3. The non-crack boundaries $M_1N_1P_1Q_1$, $M_2N_2P_2Q_2$, $M_1N_1M_2N_2$, $N_1P_1P_2N_2$, $P_1Q_1Q_2P_2$, $Q_1M_1M_2Q_2$ are discretized into a mesh system with 250 eight-node isoparametric elements and 752 nodes. The square crack is discretized as the same as that in the Section 3 for the square crack in an infinite space.

In order to plot the values of the SIFs along the crack front lines (Figs. 4–9), a line coordinate L is used to measure the crack front lines from AB, BC, CD to DA (Fig. 1). The line coordinate L starts at the corner point A of the square crack (i.e., $L/c = 0$). It increases along the lines AB, BC, CD to DA. Correspondingly, L/c increases from 0–2, from 2–4, from 4–6, and from 6–8, respectively.

4.2.2. General results

Theoretically, it can be derived that the inclined square crack in the cubic material has the SIF $K_{\mathrm{I}}(x',y',z')$ for the mode I, the SIF $K_{\mathrm{II}}(x',y',z')$ for the mode II, and the SIF $K_{\mathrm{III}}(x',y',z')$ for the mode III, where $z' = 0$.

Due to symmetry in loading, material property and geometry, the following results are valid:

$$K_{\mathrm{I}}(x', -c, 0) = K_I(x', c, 0), \tag{22a}$$

Table 2
Material combination cases of two joined transversely isotropic solids

Case no.	$z \geqslant 0^+$	$z \leqslant 0^-$	Note
1	Rhenium	Rhenium	A homogeneous transversely isotropic solid
2	Cadmium	Cadmium	A homogeneous transversely isotropic solid
3	Rhenium	Cadmium	Two joined transversely isotropic solids
4	Cadmium	Rhenium	Two joined transversely isotropic solids

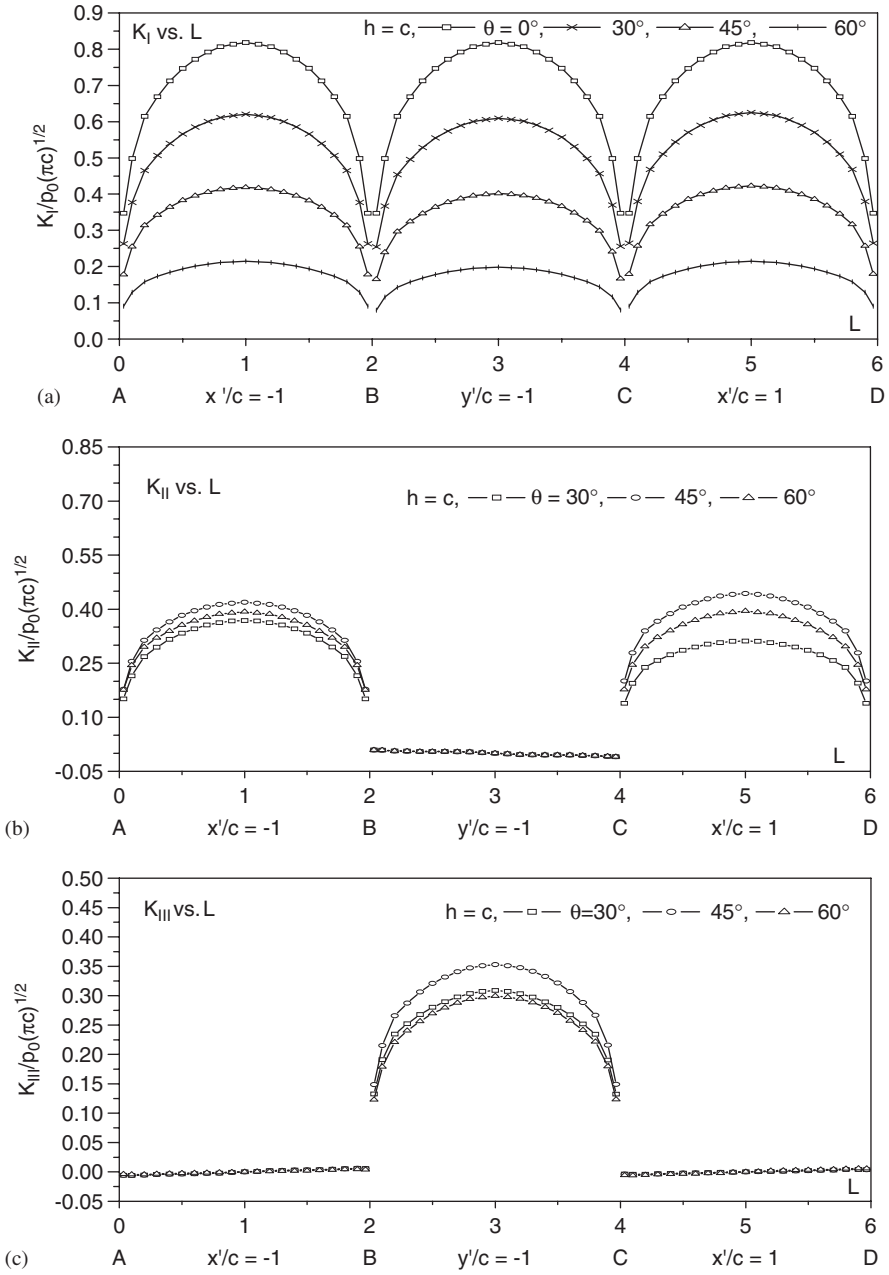

Fig. 4. SIF values of the inclined square crack along the crack front lines from AB, BC to CD in a cubic rhenium (case 1).

$$K_{\mathrm{II}}(x', -c, 0) = K_{\mathrm{II}}(x', c, 0) = 0, \tag{22b}$$

$$K_{\mathrm{III}}(x', -c, 0) = K_{\mathrm{III}}(x', c, 0), \tag{22c}$$

$$K_{\mathrm{III}}(c, y', 0) = K_{\mathrm{III}}(-c, y', 0) = 0. \tag{22d}$$

It is, therefore, that the results along the crack front line DA (i.e., $6 < L/c < 8$) are not plotted in the Figs. 4–9. Besides, if $\theta = 0^\circ$, the following results are valid:

$$K_{\mathrm{I}}(x', y', 0) \neq 0, \tag{23a}$$

$$K_{\mathrm{II}}(x', y', 0) = 0, \tag{23b}$$

$$K_{\mathrm{III}}(x', y', 0) = 0. \tag{23c}$$

Moreover, if $\theta = 90^\circ$, the following results are valid:

$$K_{\mathrm{I}}(x', y', 0) = 0, \tag{24a}$$

$$K_{\mathrm{II}}(x', y', 0) = 0, \tag{24b}$$

$$K_{\mathrm{III}}(x', y', 0) = 0. \tag{24c}$$

In addition, the numerical calculations give the values of $K_{\mathrm{II}}(x', -c, 0)$ and $K_{\mathrm{II}}(x', c, 0)$ at the 42 integral points along the crack front lines BC and DA. For all calculated results presented in Figs. 4–9, $K_{\mathrm{II}}(x', \pm c, 0)/p_0\sqrt{\pi c}$ have their values between -0.00928 and 0.00929 and have the average value 8.95×10^{-5}. This average value is almost equal to the theoretical value 0.

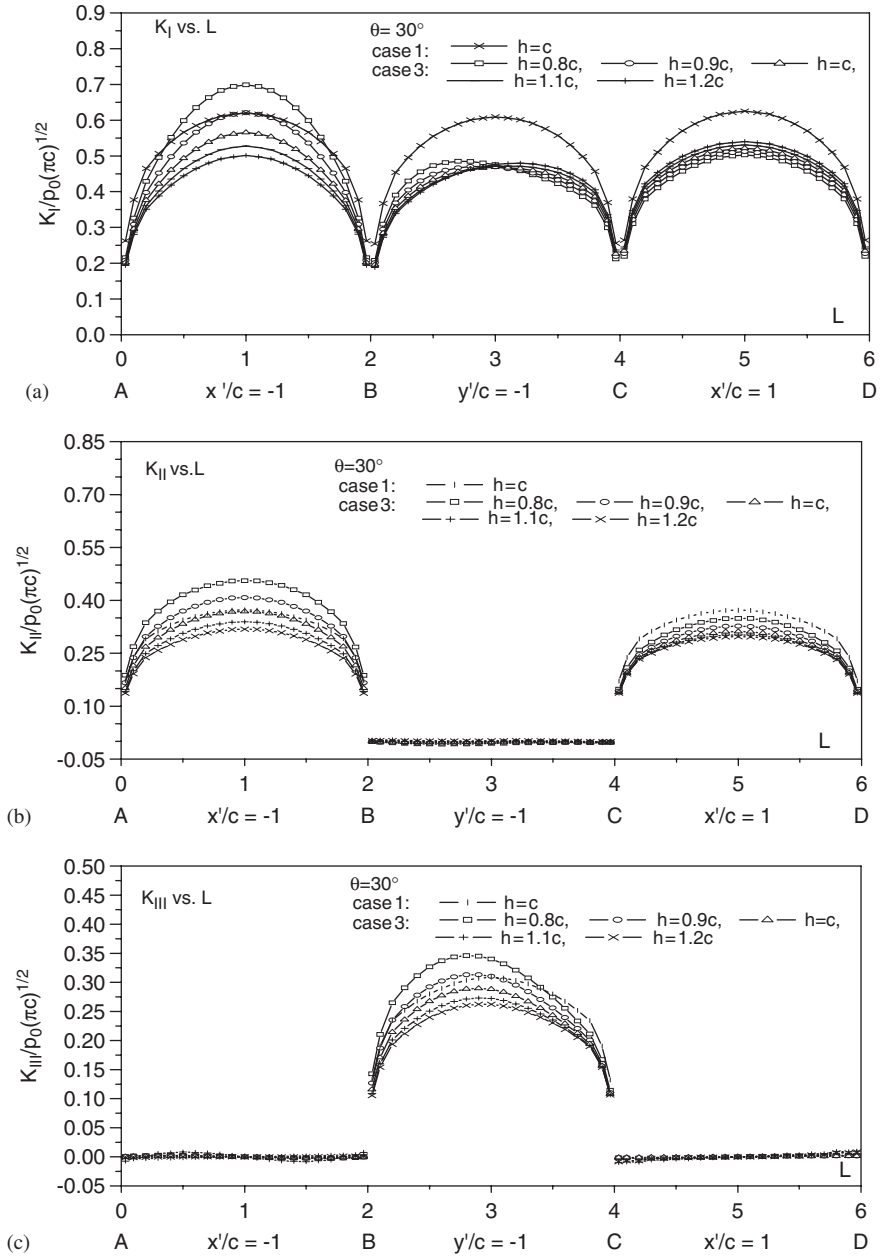

Fig. 5. SIF values of the inclined square crack with $\theta = 30^\circ$ along the crack front lines from AB, BC to CD in the cubic rhenium (case 1) or the cubic bi-material case 3.

Similarly, the numerical calculations give the values of $K_{III}(-c,y',0)$ and $K_{III}(c,y',0)$ at the 42 integral points along the crack front lines AB and CD. For all calculated results presented in Figs. 4–9, $K_{III}(\pm c,y',0)/p_0\sqrt{\pi c}$ have their values between -0.00561 and 0.00561 and have the average value -3.52×10^{-7}. This average value is almost equal to the theoretical value 0.

4.2.3. A square crack with different θ in homogeneous material

In this section, both the materials 1 and 2 in Fig. 1 are assumed to be rhenium (case 1 in Table 2). The crack problem is degenerated to an inclined square crack in a homogenous transversely isotropic solid of cubic extent. This degenerated crack problem can also be used to further verify the accuracy of the present DBEM.

If $\theta = 0^\circ$ and $h = 0$, the crack surface becomes parallel to the top and bottom surfaces of the cube. The maximum SIF value ($K_I/p_0\sqrt{\pi c}$) along the square side in the finite cube is calculated to be 0.8180. This value is well comparable to the value 0.8183 given in [4].

Fig. 4 shows the numerical results for $K_I/p_0\sqrt{\pi c}$, $K_{II}/p_0\sqrt{\pi c}$, and $K_{III}/p_0\sqrt{\pi c}$ associated with the crack along the line coordinate L/c at $\theta = 0$, 30°, 45° or 60°. From Fig. 4, the following can be observed:

- At any given crack front point $(x',y',0)$, $K_I/p_0\sqrt{\pi c}$ decrease as θ increases from 0, 30°, 45° to 60° (Fig. 4a).

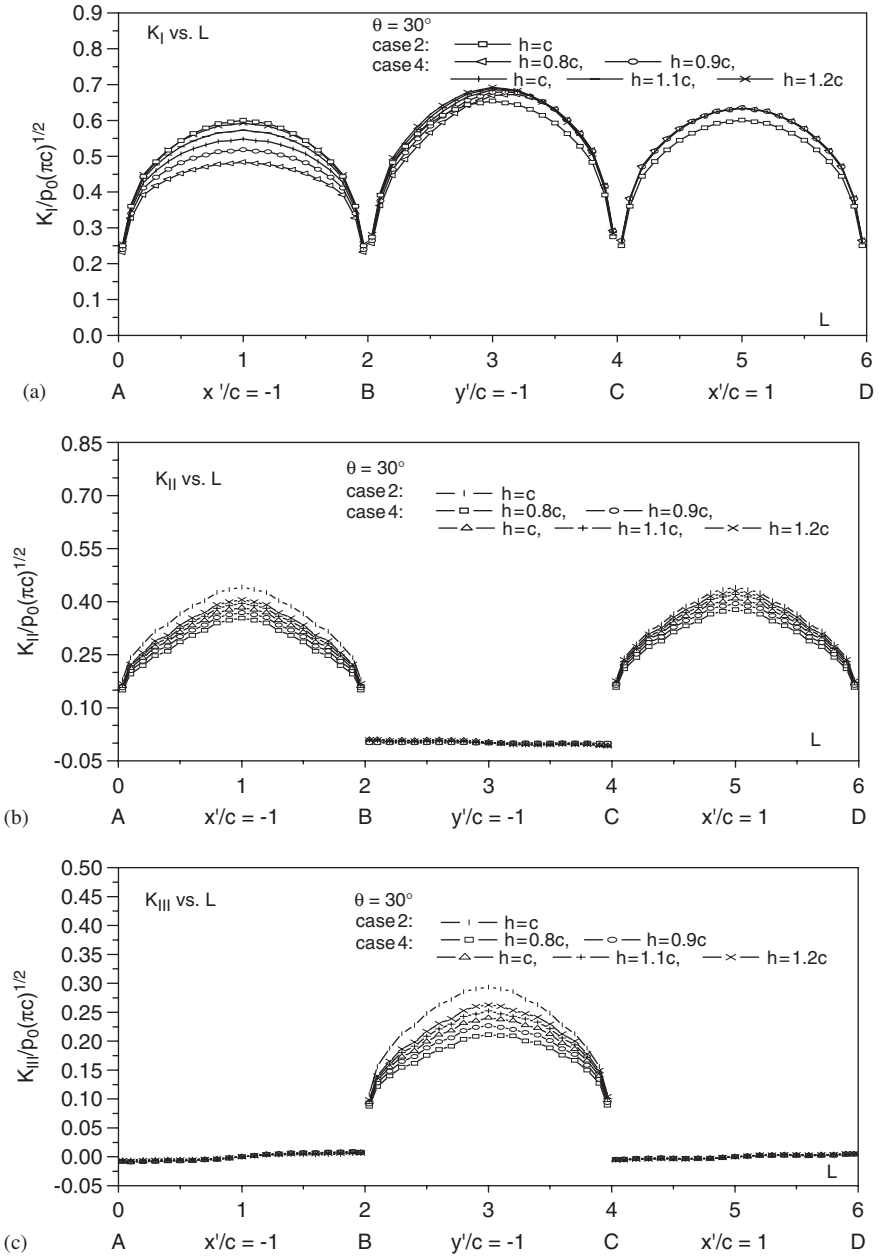

Fig. 6. SIF values of the inclined square crack with $\theta = 30^\circ$ along the crack front lines from AB, BC to CD in the cubic cadmium (case 2) or the cubic bi-material case 4.

- At any given crack front point $(\pm c, y', 0)$, $K_{\mathrm{II}}/p_0\sqrt{\pi c}$ increases as θ increases from 30°–45° while it decreases as θ increases from 45–60° (Fig. 4b).
- At any given crack front point $(x', -c, 0)$, $K_{\mathrm{III}}/p_0\sqrt{\pi c}$ increases as θ increases from 30°–45° while it decreases as θ increases from 45–60°.
- For any given θ, $K_{\mathrm{I}}/p_0\sqrt{\pi c}$ monotonically increases as L/c increases from 0–1, reach its peak at the center point $L/c = 1$, and monotonically decreases as L/c increases from 1–2 along the crack front line AB. Similar results are also found along the crack front lines BC or CD.
- For any given θ, $K_{\mathrm{II}}/p_0\sqrt{\pi c}$ monotonically increases as L/c increases from 0–1, reach its peak at the center point $L/c = 1$, and monotonically decreases as L/c increases from 1–2 along the crack front line AD. Similar results are also found along the crack front line CD.
- For any given θ, $K_{\mathrm{III}}/p_0\sqrt{\pi c}$ monotonically increases as L/c increases from 2–3, reach its peak at the center point $L/c = 3$, and monotonically decreases as L/c increases from 3–4 along the crack front line BC.
- For $\theta = 30^\circ$, the peak values of $K_{\mathrm{I}}/p_0\sqrt{\pi c}$ are 0.6252, 0.6093 and 0.6202 at $L/c = 1$, 3 and 5, respectively. The differences in $K_{\mathrm{I}}/p_0\sqrt{\pi c}$ along the crack front lines AB, BC and CD can be due to the rhenium anisotropy $E_x/E_z = 0.8032$.

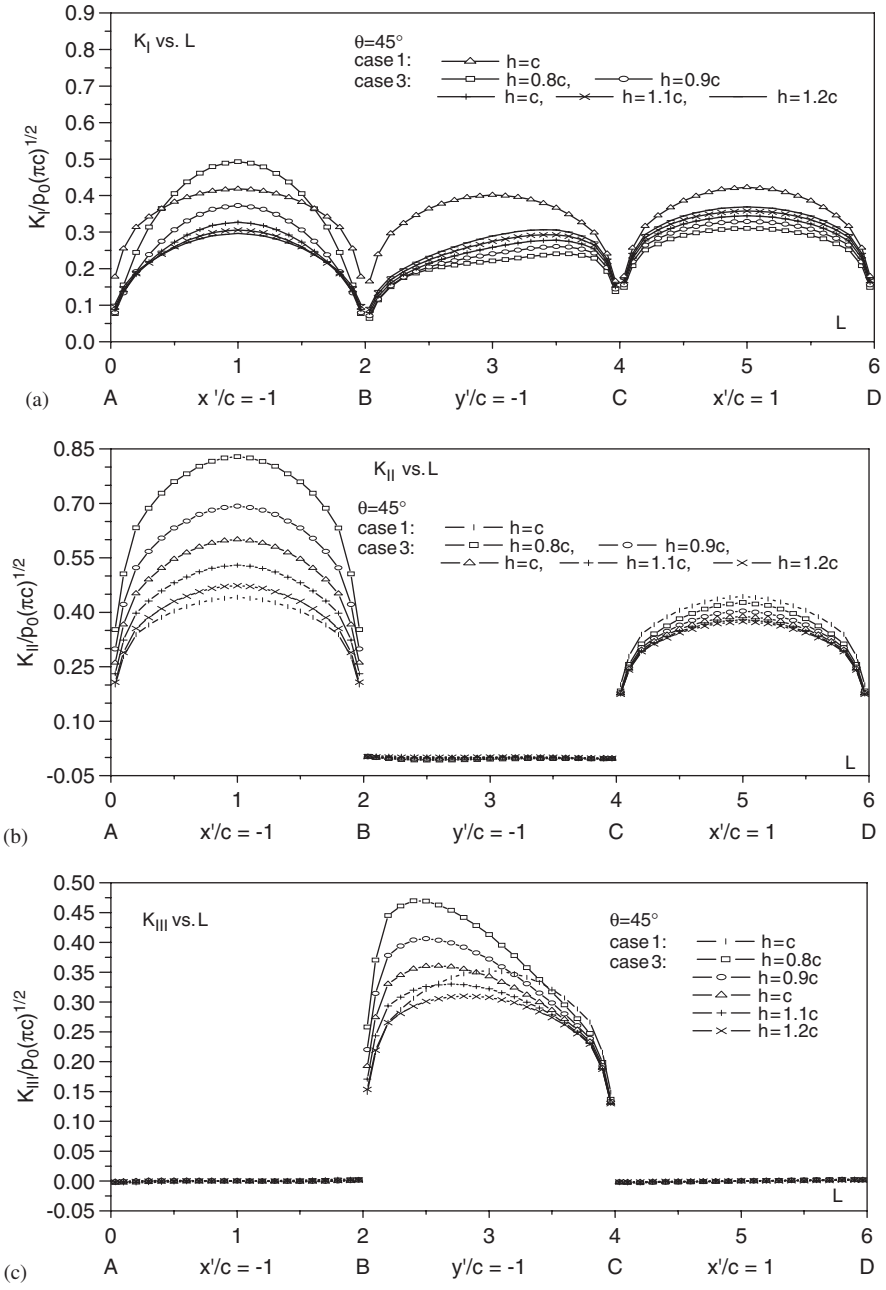

Fig. 7. SIF values of the inclined square crack with $\theta = 45^\circ$ along the crack front lines from AB, BC to CD in the cubic rhenium (case 1) or the cubic bi-material case 3.

4.2.4. A square crack with $\theta = 30^\circ$ in bi-material

In this section, the four cases of the bi-material combination in Table 2 are examined for the square crack inclined at $\theta = 30^\circ$. The calculated values of the $K_I/p_0\sqrt{\pi c}$, $K_{II}/p_0\sqrt{\pi c}$, and $K_{III}/p_0\sqrt{\pi c}$ along the crack front lines AB, BC, and CD are plotted against the line coordinate L/c in Figs. 5 and 6. The depth h of the inclined square crack is assumed to be c for the homogeneous material cases 1 and 2 and to be $0.8c$, $0.9c$, c, $1.1c$, and $1.2c$, respectively, for the bi-material cases 3 and 4. Some of the calculated values are selected in Table 3 for future comparison.

As shown in Table 2, for case 1, the material 1 where the crack is located is rhenium and is the same as material 2. For case 3, material 1 where the crack is located is rhenium and is stiffer than material 2 (cadmium). Figs. 5a–c show the calculated results for the values of $K_I/p_0\sqrt{\pi c}$, $K_{II}/p_0\sqrt{\pi c}$, and $K_{III}/p_0\sqrt{\pi c}$ along the line coordinate L/c, respectively. From Fig. 6, the following can be observed:

- For $h = c$, the differences in the SIF values between the cases 1 and 3 are mainly due to the different property for the material 2. For each given L/c, the values of $K_I/p_0\sqrt{\pi c}$, $K_{II}/p_0\sqrt{\pi c}$, and $K_{III}/p_0\sqrt{\pi c}$ for the case 1 are greater than those for the case 3, respectively. This result has shown that a softer material 2 can cause a reduction in the SIF values in the bi-materials.

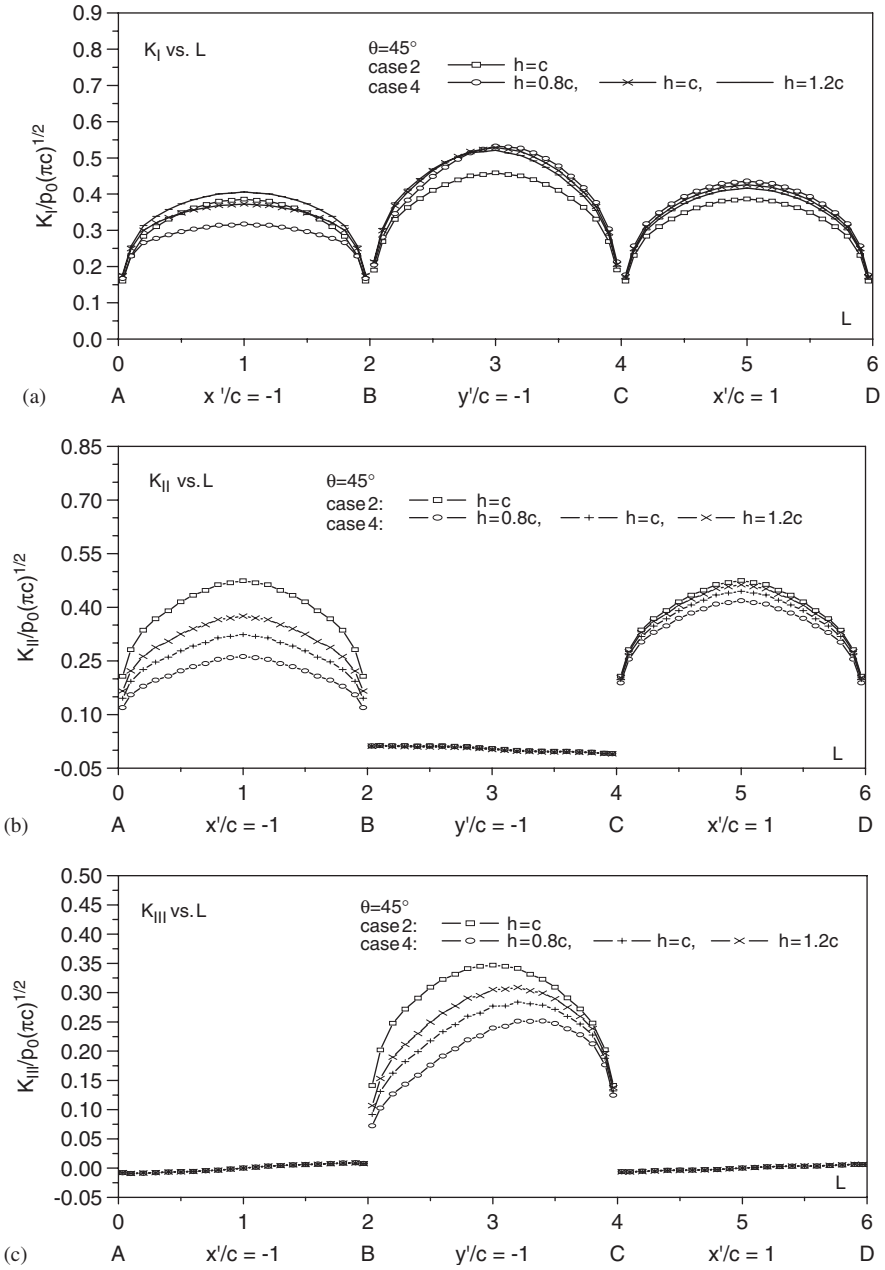

Fig. 8. SIF values of the inclined square crack with $\theta = 45^\circ$ along the crack front lines from AB, BC to CD in the cubic cadmium (case 2) or the cubic bi-material case 4.

- For each given L/c, the values of $K_I/p_0\sqrt{\pi c}$, $K_{II}/p_0\sqrt{\pi c}$, and $K_{III}/p_0\sqrt{\pi c}$ associated with the case 3 gradually increase as the depth h decreases from $1.2c$–$0.8c$.
- In particular, when $0.4 < L/c < 1.6$, $K_I/p_0\sqrt{\pi c}$ for case 3 at $h = 0.8c$ can be greater than the corresponding value for case 1 at $h = c$. Similarly, when $0 < L/c < 2$, $K_{II}/p_0\sqrt{\pi c}$ for case 3 at $h = 0.8c$ or $h = 0.9c$ can be greater than the corresponding value for case 1 at $h = c$. When $2 < L/c < 4$, $K_{III}/p_0\sqrt{\pi c}$ for case 3 at $h = 0.8c$ or $h = 0.9c$ can be greater than the corresponding value for case 1 at $h = c$. These results are due to the presence of softer material 2.

Similarly, as shown in Table 2, for case 2, material 1 where the crack is located is cadmium and is the same as material 2. For case 4, material 1 where the crack is located is cadmium and is softer than material 2 (rhenium). Figs. 6a–c show the calculated results for the values of $K_I/p_0\sqrt{\pi c}$, $K_{II}/p_0\sqrt{\pi c}$, and $K_{III}/p_0\sqrt{\pi c}$ along the line coordinate L/c, respectively. From Fig. 6, the following can be observed:

- For $h = c$, the differences in the SIF values between cases 2 and 4 are mainly due to the different property for material 2. The differences are shown in Fig. 6.

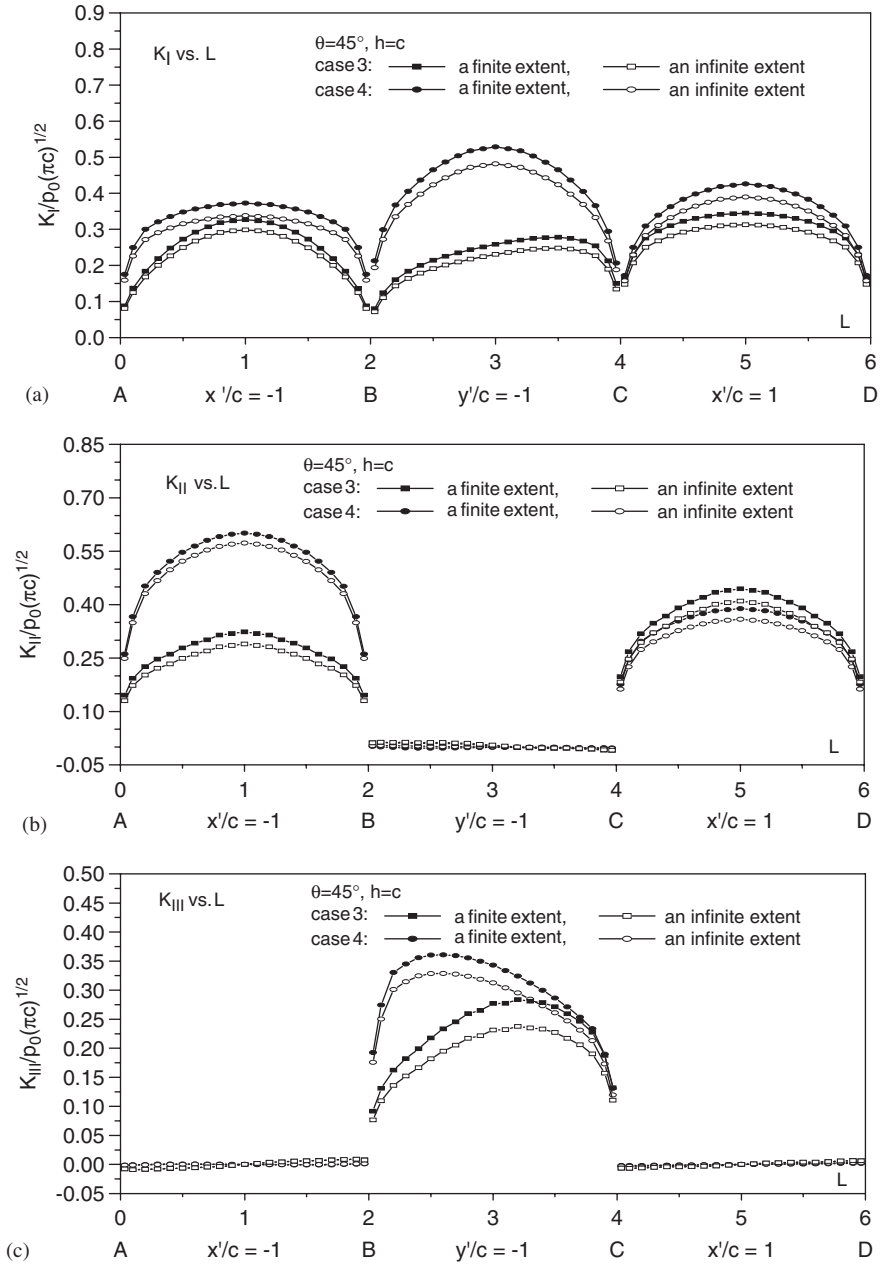

Fig. 9. SIF values of the inclined square crack with $\theta = 45^\circ$ along the crack front lines from AB, BC to CD in the bi-material cases 3 or 4 occupying a cubic or infinite space.

Table 3
Selected SIF values of the square crack in a cubic bi-material along $x'/c = -1$ at $\theta = 30^\circ$ and $h = c$

y'/c	$K_I/p_0\sqrt{\pi c}$				$K_{II}/p_0\sqrt{\pi c}$			
	Case 1	Case 2	Case3	Case 4	Case 1	Case 2	Case 3	Case 4
−0.9	0.3770	0.3600	0.2960	0.3507	0.2387	0.2413	0.2149	0.2119
−0.7	0.5067	0.4846	0.4218	0.4604	0.3124	0.3163	0.2942	0.2716
−0.5	0.5661	0.5437	0.4934	0.5063	0.3443	0.3655	0.3331	0.3134
−0.3	0.6001	0.5785	0.5388	0.5316	0.3628	0.4031	0.3560	0.3470
−0.1	0.6165	0.5954	0.5615	0.5436	0.3720	0.4342	0.3672	0.3765
0.0	0.6201	0.6004	0.5657	0.5480	0.3728	0.4405	0.3683	0.3827

- As shown in Fig. 6a, as L/c increases from 0–6, $K_I/p_0\sqrt{\pi c}$ associated with case 4 becomes less and less changeable as the depth h decreases. For $0<L/c<2$, $K_I/p_0\sqrt{\pi c}$ associated with case 4 clearly shows that the depth h decreases from $1.2c$–$0.8c$. Besides, when $0<L/c<2$, the $K_I/p_0\sqrt{\pi c}$ associated with case 4 for $0.8c\leqslant h\leqslant 1.2c$ is less than that associated with case 2. But, when $2<L/c<6$, $K_I/p_0\sqrt{\pi c}$ associated with case 4 for $0.8c\leqslant h\leqslant 1.2c$ becomes greater than that associated with case 2 for $h=c$.
- As shown in Fig. 6b, $K_{II}/p_0\sqrt{\pi c}$ associated with case 4 decreases as the depth h decreases from $1.2c$–$0.8c$ and is less than that associated with case 2 for $h=c$, where $0<L/c<2$ or $4<L/c<6$.
- As shown in Fig. 6c, $K_{III}/p_0\sqrt{\pi c}$ associated with case 4 decreases as the depth h decreases from $1.2c$–$0.8c$ and is less than that associated with case 2 for $h=c$, where $2<L/c<4$.

Based on the above analysis, it can be concluded that for the crack in a stiffer material 1, the softer material 2 tends to increase the magnitude of the SIFs along the crack front. For the crack in a softer material 1, the stiffer material 2 tends to reduce the magnitude of the SIFs along the crack front. However, K_I along the crack front lines BC and CD can have different variation patterns with respect to the relative stiffness of the materials 1 and 2.

4.2.5. A square crack with $\theta=45^\circ$ in bi-material

In this section, the four cases of the bi-material combination in Table 2 are examined for the square crack inclined at $\theta=45^\circ$. The calculated values of the $K_I/p_0\sqrt{\pi c}$, $K_{II}/p_0\sqrt{\pi c}$, and $K_{III}/p_0\sqrt{\pi c}$ along the crack front lines AB, BC, and CD are plotted against the line coordinate L/c in Figs. 7 and 8. The depth h of the inclined square crack is assumed to be c for the homogeneous material cases 1 and 2 and to be $0.8c$, $0.9c$, c, $1.1c$, and $1.2c$, respectively, for the bi-material cases 3 and 4. Some of the calculated values are selected in Table 4 for future comparison.

Similar observations as those discussed in Section 4.2.4 for $\theta=30^\circ$ can be found from Figs. 7 and 8 for $\theta=45^\circ$. Furthermore, the effect of the inclination angle θ of the square crack on its SIF values in the bi-material cube can be found by comparing the results in Figs. 5 and 6 with those corresponding results in Figs. 7 and 8. Basically, $K_I/p_0\sqrt{\pi c}$ for $\theta=45^\circ$ becomes smaller than that for $\theta=30^\circ$. $K_{II}/p_0\sqrt{\pi c}$ and $K_{III}/p_0\sqrt{\pi c}$ for $\theta=45^\circ$ become much larger than those for $\theta=30^\circ$.

4.3. A square crack in a transversely isotropic bi-material of infinite space

In this section, a square crack in a transversely isotropic bi-material of infinite space is examined. The objective of this examination is to study the effect of the external non-crack boundary on the SIF values. The effect is found by comparing the SIF values for the square crack in the finite cubic bi-material with those in the bi-material occupying an infinite space.

The square crack is shown in Fig. 1, where the external boundaries points M_1, N_1, P_1, Q_1, M, N, P, Q, M_2, N_2, P_2, and Q_2 are extended to infinite. $\theta=45^\circ$ and $h=c$. The square crack surfaces Γ^+ ($z'=0^+$) and Γ^- ($z'=0^-$) are subject to a uniform tension p_0 along the z-axis. The bi-materials are the cases 3 and 4 in Table 2. The crack surface mesh in Fig. 3 is further used.

Figs. 9a–c show the calculated results of $K_I/p_0\sqrt{\pi c}$, $K_{II}/p_0\sqrt{\pi c}$, and $K_{III}/p_0\sqrt{\pi c}$ with respect to the line coordinate L/c along the crack front lines AB, BC, and CD in either the cubic bi-materials or the infinite bi-materials. From Fig. 9, the following can be observed:

- The variation patterns of the $K_I/p_0\sqrt{\pi c}$, $K_{II}/p_0\sqrt{\pi c}$, and $K_{III}/p_0\sqrt{\pi c}$ with respect to the line coordinate L/c are similar for both the cubic and the infinite bi-materials, which indicate that the external non-crack boundary does not have effect on the variation patterns.
- However, for each L/c, the calculated values of $K_I/p_0\sqrt{\pi c}$, $K_{II}/p_0\sqrt{\pi c}$, and $K_{III}/p_0\sqrt{\pi c}$ for the crack in the infinite bi-material are slightly less than those in the finite cubic bi-materials.
- In particular, for $0<L/c<2$ or on the crack front line AB ($x'/c=-1$),$K_I/p_0\sqrt{\pi c}$ has its maximum value as follows: (a) 0.3268 for the cubic bi-material case 3; (b) 0.2988 for the infinite bi-material case 3; (c) 0.3729

Table 4
Selected SIF values of the square crack in a cubic bi-material along $x'/c=-1$ at $\theta=45^\circ$ and $h=c$

y'/c	$K_I/p_0\sqrt{\pi c}$				$K_{II}/p_0\sqrt{\pi c}$			
	Case 1	Case 2	Case3	Case 4	Case 1	Case 2	Case 3	Case 4
−0.9	0.2547	0.2304	0.1366	0.2495	0.2777	0.2812	0.3661	0.1928
−0.7	0.3423	0.3100	0.2191	0.3206	0.3649	0.3679	0.4902	0.2470
−0.5	0.3825	0.3484	0.2728	0.3478	0.4036	0.4149	0.5470	0.2783
−0.3	0.4055	0.3715	0.3072	0.3628	0.4266	0.4472	0.5804	0.3014
−0.1	0.4164	0.3828	0.3239	0.3700	0.4385	0.4687	0.5976	0.3185
0.0	0.4187	0.3862	0.3268	0.3729	0.4412	0.4744	0.6007	0.3233

for the cubic bi-material case 4; and (d) 0.3379 for the infinite bi-material case 4.

- In particular, for $0<L/c<2$ or on the crack front line AB ($x'/c=-1$),$K_{II}/p_0\sqrt{\pi c}$ has its maximum value as follows: (a) 0.6007 for the cubic bi-material case 3; (b) 0.5730 for the infinite bi-material case 3; (c) 0.3233 for the cubic bi-material case 4; and (d) 0.2893 for the infinite bi-material case 4.

The findings in the above can indicate that the larger the external boundary of the cracked bi-material, the higher the constraint of the external boundary of the crack bi-material on the opening and sliding of the square crack.

5. Summary and conclusions

In the above, a new DBEM has been proposed and examined. This method incorporates the fundamental solutions for two joined transversely isotropic solids into the existing DBEM. A square crack in a transversely isotropic bi-material of either finite or infinite extent is investigated in detail. Two transversely isotropic materials are considered. Four cases of the transversely isotropic bi-materials are used for the calculation of the SIF values associated with the square crack along the four crack front lines. The numerical results have shown that the material anisotropy and the bi-material properties have clear effects on the SIF values. The SIF values along the crack front lines in a bi-material can be different with those in a homogeneous material. Such difference can become substantial when the crack front is adjacent the interface of the bi-material. The SIFs for a square crack in an infinite bi-material are also calculated and compared to those in the corresponding bi-materials with finite cubic space. The external boundary of the cracked bi-material cube can have some effects on the magnitude of the SIFs but has negligible effect on the variation patterns of the SIFs along the crack front lines.

Acknowledgments

The authors would like to thank the financial supports from the Research Grants Council of Hong Kong SAR Government. The author E. Pan thanks the Faculty of Engineering, The University of Hong Kong, for the William Mong Visiting Research Fellowship in Engineering in 2005.

Appendix A

For a transversely isotropic bi-material solid with the z-axis being the axis of material symmetry, x-y plane is the plane of isotropy, as shown in Fig. 1. The constitutive relation between the stresses σ_{ij} and the strains ε_{ij} can be expressed in terms of the following matrix as

$$\begin{bmatrix}\sigma_{xx}\\ \sigma_{yy}\\ \sigma_{zz}\\ \sigma_{yz}\\ \sigma_{xz}\\ \sigma_{xy}\end{bmatrix} = \begin{bmatrix} c_{1k} & c_{1k}-2c_{5k} & c_{2k} & 0 & 0 & 0\\ c_{1k}-2c_{5k} & c_{1k} & c_{2k} & 0 & 0 & 0\\ c_{2k} & c_{2k} & c_{3k} & 0 & 0 & 0\\ 0 & 0 & 0 & 2c_{4k} & 0 & 0\\ 0 & 0 & 0 & 0 & 2c_{4k} & 0\\ 0 & 0 & 0 & 0 & 0 & 2c_{5k}\end{bmatrix} \times \begin{bmatrix}\varepsilon_{xx}\\ \varepsilon_{yy}\\ \varepsilon_{zz}\\ \varepsilon_{yz}\\ \varepsilon_{xz}\\ \varepsilon_{xy}\end{bmatrix}, \tag{A1}$$

where c_{1k}, c_{2k}, c_{3k}, c_{4k}, and c_{5k} are the five elastic constants for the kth transversely isotropic solid of the bi-material system, where $k=1$ for $0^+\leqslant z<\infty$ or 2 for $-\infty<z\leqslant 0^-$.

References

[1] Sih GC, Paris PC, Irwin GR. On crack in rectilinearly anisotropic bodies. Int J Fract 1965;1:189–203.
[2] Sih GC, Chen EP. Cracks in composite materials: a compilation of stress solutions for composite systems with cracks. The Hague: Nijhoff; 1981.
[3] Hoenig A. The behavior of a flat elliptical crack in an anisotropic elastic body. Int J Solids Struct 1978;14:925–34.
[4] Pan E, Yuan FG. Boundary element analysis of three-dimensional crack in anisotropic solids. Int J Numer Meth Eng 2000;48:211–37.
[5] Qin TY, Noda NA. Stress intensity factors of a rectangular crack meeting a bimaterial interface. Int J Solids Struct 2003;40:2473–86.
[6] Xiao HT, Yue ZQ, Tham LG, Lee CF. Analysis of elliptical cracks perpendicular to the interface of two joined transversely isotropic solids. Int J Fract 2005;133:329–54.
[7] Yue ZQ, Xiao HT, Tham LG, Lee CF, Pan E. Boundary element analysis of 3D crack problems in two joined transversely isotropic solids. Comput Mech 2005;36:459–74.
[8] Yue ZQ. Elastic fields in two joined transversely isotropic solids due to concentrated forces. Int J Eng Sci 1995;33:351–69.
[9] Mi Y, Aliabadi MH. Dual boundary element method for three-dimensional fracture mechanics analysis. Eng Bound Elem 1992;10:161–71.
[10] Portela A, Aliabadi MH, Rooke DP. Dual boundary element method: efficient implementation for cracked problems. Int J Numer Meth Eng 1992;33:1269–87.
[11] Pan YC, Chou TW. Point force solution for an infinite transversely isotropic solid. ASME J Appl Mech 1976;43:608–12.

[12] Ariza MP, Dominguez J. Boundary element formulation for 3D transversely isotropic cracked bodies. Int J Numer Meth Eng 2004;60: 719–53.
[13] Pan E, Amadei B. Fracture mechanics analysis of cracked 2D anisotropic media with a new formulation of boundary element method. Int J Fract 1996;77:161–74.
[14] Pan E. A general boundary element analysis of 2-D linear elastic fracture mechanics. Int J Fract 1997;88:41–59.
[15] Wilde A. A dual boundary element formulation for 3D fracture analysis. Southampton, UK: WIT Press; 2000.
[16] Tonon F, Pan E, Amadei B. Green's functions and boundary element method formulation for 3D anisotropic media. Comput Struct 2001;79:469–82.
[17] Crouch SL, Starfield AM. Boundary element methods in solid mechanics. London: George Allen and Unwin Publishers; 1983.
[18] Weaver J. Three-dimensional crack analysis. Int J Solids Struct 1977; 13:321–30.
[19] Cisilino A. Linear and nonlinear crack growth using boundary elements. Southampton, UK: WIT Press; 2000.
[20] Lachat JC, Watson JO. Effective treatment of boundary integral equations: a formulation for three-dimensional elastostatics. Int J Numer Meth Eng 1976;10:991–1005.
[21] Gao XW, Davies TG. Boundary element programming in mechanics. Cambridge University; 2002.
[22] Yue ZQ, Xiao HT. Generalized Kelvin solution based boundary element method for crack problems in multilayered solids. Eng Anal Bound Elem 2002;26:691–705.
[23] Kutt HR. Quadrature formulae for finite-part integrals. Special report WISK 178, National Research Institute for Mathematical Sciences, Pretoria, 1975.
[24] Kutt HR. On the numerical evaluation of finite-part integrals involving an algebraic singularity. Special report WISK 179, National Research Institute for Mathematical Sciences, Pretoria, 1975.
[25] Kassir MK, Sih GC. Three-dimensional stress distribution around an elliptical crack under arbitrary loadings. ASME J Appl Mech 1966; 33:601–11.
[26] Ting TCT. Anisotropic elasticity: theory and applications. New York: Oxford University Press; 1996.
[27] Murakami Y. Stress intensity factors handbook. Oxford: Pergamon Press; 1987.
[28] Lin W, Keer LM. Three-dimensional analysis of cracks in layered transversely isotropic media. Proc R Soc (London) 1989;A424: 307–22.